Cite as: H. Kim *et al.*, *Science* 10.1126/science.aam8743 (2017).

Water harvesting from air with metal-organic frameworks powered by natural sunlight

Hyunho Kim,[1] Sungwoo Yang,[1] Sameer R. Rao,[1] Shankar Narayanan,[1]* Eugene A. Kapustin,[2] Hiroyasu Furukawa,[2] Ari S. Umans,[1] Omar M. Yaghi,[2,3]† Evelyn N. Wang[1]†

[1]Department of Mechanical Engineering, Massachusetts Institute of Technology, 77 Massachusetts Avenue, Cambridge, MA 02139, USA. [2]Department of Chemistry, University of California–Berkeley; Materials Sciences Division, Lawrence Berkeley National Laboratory; Kavli Energy NanoSciences Institute at Berkeley; Berkeley Global Science Institute; Berkeley, CA 94720, USA. [3]King Abdulaziz City for Science and Technology, Riyadh 11442, Saudi Arabia.

***Present address: Department of Mechanical, Aerospace and Nuclear Engineering, Rensselaer Polytechnic Institute, 110 8th Street, Troy, NY 12180, USA.**

†Corresponding author. Email: yaghi@berkeley.edu (O.M.Y.); enwang@mit.edu (E.N.W.)

Atmospheric water is a resource equivalent to ~10% of all fresh water in lakes on Earth. However, an efficient process for capturing and delivering water from air, especially at low humidity levels (down to 20%), has not been developed. We report the design and demonstration of a device based on porous metal-organic framework-801 [$Zr_6O_4(OH)_4(fumarate)_6$] that captures water from the atmosphere at ambient conditions using low-grade heat from natural sunlight below one sun (1 kW per square meter). This device is capable of harvesting 2.8 liters of water per kilogram of MOF daily at relative humidity levels as low as 20%, and requires no additional input of energy.

Two-thirds of the world's population is experiencing water shortages (*1*). The water vapor and droplets in the atmosphere, estimated to be around 13,000 trillion liters (*2*), is a natural resource that could address the global water problem. Although there has been interest in dewing (*3*–*6*) from moist air and fog capture (*7*–*9*), these processes require either frequent presence of 100% relative humidity (RH) or a large amount of energy, and are not viable solutions to the capture of water from air. Ideally, a water-harvesting system should operate with a material that can take up and release water with minimum energy requirements and powered by low-grade energy sources, such as sunlight, in order to potentially allow its deployment into households, especially those located in sunny regions. Here, we demonstrate water harvesting by vapor adsorption using a porous metal-organic framework (microcrystalline powder MOF-801, [$Zr_6O_4(OH)_4(fumarate)_6$]) (*10*) in ambient air with low RH, typical of the levels found in most dry regions of the world (down to RH of 20%). We also report a device based on this MOF that can harvest and deliver water (2.8 L kg^{-1} day^{-1} at 20% RH) under a non-concentrated solar flux below 1 sun (1 kW m^{-2}), requiring no additional power input for producing water at ambient temperature outdoors.

Porous materials, such as zeolites, silica gels, and MOFs, can harvest water from air by adsorption over a wide range of humidity values (*11*–*13*). However, these materials suffer from either low uptake of water or high energy consumption for its release. Although MOFs have already been considered in numerous applications, including gas storage, separation, and catalysis (*14*–*16*), heat pump (*17*, *18*), and dehumidification (*19*), the use of MOFs for water harvesting has only recently been proposed (*10*). The flexibility (*20*–*22*) with which MOFs can be made and modified at the molecular level coupled to their ultra-high porosity make them ideally suited for overcoming the challenges mentioned above.

A critical step is the release of water from the MOF, for which we applied a low-grade heat driven (*23*, *24*) vapor desorption process. Solar energy is particularly promising because sunlight is often abundant in arid regions with low RH (> 7 kWh m^{-2} day^{-1}, equivalent to 7 hours of 1 sun per day) where water resources are limited and where a natural diurnal temperature swing thermally assists the process (adsorption of water during the cooler night and release during the warmer day). This strategy is much more energy efficient compared to refrigeration-based dew harvesting systems because heat is directly used for desorption. The amount of water that can be harvested with MOFs can be much greater than dew harvesting systems, which become impractical at RHs < 50% (*25*).

To harvest water using MOFs with maximum yield and minimal energy consumption, an isotherm with a steep increase in water uptake within a narrow range of RH is desired, which enables maximum regeneration with minimal temperature rise. Recent MOFs have exhibited such sorption characteristics (Fig. 1A). In particular, MOF-801 is suitable for regions where RH is merely 20% (e.g., North Africa), and UiO-66 (*10*, *26*) is suitable for regions with ~40% RH (e.g., Northern India). We harvested water with MOF-801 and natural sunlight < 1 sun in an environment at regeneration temperatures of ~65°C. Once water vapor ad-

sorbed into the MOF, solar energy was used to release the adsorbate. Water was then harvested using a condenser maintained at temperatures near the surrounding environment. For MOF-801, a temperature swing between 25°C and 65°C can harvest over 0.25 L kg^{-1} of water above 0.6 kPa vapor pressure (20% RH at 25°C, Fig. 1B). This water harvesting strategy is completely passive, relying only on the high water uptake capacity, low-grade heat requirement for desorption, and ambient to condense and collect the water. (Fig. 1C).

For our approach, MOF-801 has several advantages in that it has: (i) well-studied water adsorption behavior on a molecular level; (ii) good performance driven by aggregation of water molecules into clusters within the pores of the MOF; (iii) exceptional stability and recycling; and (iv) wide availability and low cost of its constituents. It is composed of 12-connected Zr-based clusters $Zr_6O_4(OH)_4(\text{-}COO)_{12}$ joined by fumarate linkers into a three-dimensional, extended porous framework of **fcu** topology. The structure of MOF-801 contains three symmetrically independent cavities into which water molecules can be captured and concentrated (Fig. 1D).

We carried out the adsorption-desorption experiments for water harvesting with MOF-801 at 20% RH. A powder of MOF-801 was synthesized as reported (*10*) and then activated (solvent removal from the pores) by heating at 150°C under vacuum for 24 hours. The powder was infiltrated into a porous copper foam with a thickness of 0.41 cm and porosity of ~0.95, brazed on a copper substrate, to create an adsorbent layer (5 cm by 5 cm by 0.41 cm) with 1.79 g of activated MOF-801 with an average packing porosity of ~0.85 (Fig. 2A), with enhanced structural rigidity and thermal transport. This particular geometry with a high substrate area to thickness ratio was selected to reduce parasitic heat loss.

Experiments were performed in a RH-controlled environmental chamber interfaced with a solar simulator. The fabricated MOF-801 layer was placed in the chamber (Fig. 2A), and evacuated under high vacuum below 1 Pa at 90°C. Water vapor was then introduced inside the chamber to maintain a condition equivalent to a partial vapor pressure of 20% RH at 35°C, matching the step rise in water uptake for the MOF-801 (Fig. 1A). Vapor was adsorbed onto the sample surfaces by diffusion (Fig. 2B). After saturation, the chamber was isolated from the vapor source. A solar flux (1 kW m^{-2}, AM1.5 spectrum) was introduced to the graphite coated substrate layer with a solar absorptance of 0.91 to desorb water from the MOF. This water was then collected via a condenser interfaced with a thermoelectric cooler which maintains the isobaric conditions of ~1.2 kPa (20% RH at 35°C, saturation temperature of ~10°C). By maintaining the isobaric condition, all of the desorbed vapor was condensed and harvested by the condenser (*25*). During desorption, the water harvesting rate (or vapor desorption rate) was continuously monitored with a heat flux sensor interfaced to the condenser. The environmental temperature above standard ambient temperature was necessary to perform the experiments above 1 kPa; otherwise, a much lower condenser temperature is needed (e.g., ~0.5°C for 20% RH at 25°C). Thermocouples were placed on both sides of the MOF-801 layer to monitor the dynamic temperature response.

Figure 2C shows the temperature of the MOF-801 layer and pressure inside the chamber during the adsorption and solar-assisted desorption experiments. During adsorption, the temperature of the MOF-801 layer first rapidly increased because the exothermic adsorption process, and then slowly decreased as heat was lost to the surroundings. After ~70 min of adsorption, the MOF-801 temperature equilibrated with the surrounding vapor of ~35°C. At these given adsorption conditions, the predicted water uptake, or potential harvestable quantity of water, was estimated to be ~0.25 kg H_2O kg^{-1} MOF, as shown in the upper abscissa of Fig. 2C. For MOF-801, ~0.24 L kg^{-1} of water was harvested per each water harvesting cycle (Fig. 2D), obtained by integrating the water harvesting rate. We further confirmed the experimental result with an adsorption analyzer under identical adsorption-desorption conditions (fig. S2A).

A theoretical model was developed to optimize the design of the water harvesting process with MOF-801, which was further validated with the experimental data. The model framework was based on mass and energy conservation incorporating adsorption dynamics parameters (*27*, *28*), and the analysis was carried out by using COMSOL Multiphysics (*25*). The inter- and intracrystalline vapor diffusion through the layer and within the crystals, as well as the thermal transport through the layer, were considered in the model. The theoretical model produced good agreement with the experimental data from the water-harvesting experiment (Fig. 2, C and D). We then investigated the water harvesting behavior under ambient air conditions by incorporating the diffusion and sorption characteristics of MOF-801 at ambient conditions into the theoretical model (*25*). We performed a parametric study, including varying the packing porosity (0.5, 0.7, and 0.9) and layer thickness (1, 3, 5, and 10 mm), and determined the time and amount of harvestable water using a solar flux of 1 sun (1 kW m^{-2}) (*25*). By considering both the adsorption and desorption dynamics, a porosity of 0.7 was predicted to yield the largest quantity of water. At a porosity of ~0.5 or less, the adsorption kinetics is limited by Knudsen diffusion because the crystal diameter of MOF-801 is only ~0.6 μm (fig. S5). The characteristic void spacing for Knudsen diffusion is a function of packing porosity and the crystal diameter. However, at higher porosi-

ties, a thicker MOF-801 layer is required to harvest a sufficient amount of water, but the time scale and transport resistance for intercrystalline diffusion also scales with the MOF layer thickness as $t \sim L_c^2/D_v$, where, t, D_v, and L_c are the time scale, intercrystalline diffusivity, and characteristic length scale (i.e., layer thickness), respectively.

Simulated adsorption-desorption dynamics for the MOF-801 layer of the optimized packing porosity of 0.7 are shown in Fig. 3 for 1 sun and realistic boundary conditions for heat loss (a natural heat transfer coefficient of 10 W m^{-2} K^{-1} and standard ambient temperature). In this simulation, MOF-801 was initially equilibrated at 20% RH, and the vapor content in the air-vapor mixture that surrounds the layer during desorption increased rapidly from 20% RH to 100% RH at 25°C. This scenario is more realistic compared to the model experiment described above because water is harvested by a condenser at ambient temperature. Once solar irradiation was stopped, the air-vapor concentration reverted to 20% RH for vapor adsorption from ambient air, and the heat from the adsorption process was transferred to the surroundings. A detailed description of the boundary conditions and idealizations in the simulation are discussed in section S8 of the supplementary materials. First, water uptake decreased with time during solar heating and water condensation, and then increased through adsorption, as shown on the simulated water uptake profiles for the MOF-801 layer with a thickness of 1, 3, and 5 mm in Fig. 3. The temperature correspondingly increased and then decreased with time. Continuously harvesting water in a cyclic manner for a 24-hour period with low-grade heat at 1 kW m^{-2} can yield ~2.8 L kg^{-1} day^{-1} or ~0.9 L m^{-2} day^{-1} of water with a layer with 1 mm thickness. Alternatively, per one cycle, a 5 mm thick layer of MOF-801 can harvest ~0.4 L m^{-2} of water. Our findings indicate that MOFs with the enhanced sorption capacity and high intracrystalline diffusivity along with an optimized crystal diameter and density, and thickness of the MOF layer can boost the daily quantity of the harvested water from an arid environment.

Finally, a proof-of-concept MOF-801 water-harvesting prototype was built to demonstrate the viability of this approach outdoors (Fig. 4A). This prototype includes a MOF-801 layer (packing porosity of ~0.85, 5 cm by 5 cm and 0.31 cm thick containing 1.34 g of activated MOF), an acrylic enclosure, and a condenser, which was tested on a roof at MIT . The spacing between the layer and condenser in the prototype was chosen to be large enough to enable ease of sample installation and visualization. The activated MOF-801 layer was left on the roof overnight for vapor adsorption from ambient air (day 1). The desorption process using natural sunlight was carried out on day 2 (ambient RH was ~65% at the start of experiment). For visualization purposes, we used a condenser with a temperature controller to maintain the temperature slightly below ambient, but above the dew point, to prevent vapor condensation on the inner walls of the enclosure. However, active cooling is not needed in a practical device since the hot desorbed vapor can condense at the cooler ambient temperature using a passive heat sink.

The formation, growth and multiplication of water droplets on the condenser with the change of the MOF layer temperature and time are shown in Fig. 4B. The temperature and solar flux (global horizontal irradiation) measurements during the solar-assisted desorption process revealed a rapid increase in the MOF-801 temperature accompanied with the relatively low solar fluxes (Fig. 4C). Because water harvesting with vapor condensation is done with the presence of noncondensables (air), transport of desorbed vapor from the layer to the condenser surface is by diffusion. Using the experimentally measured solar flux and environmental conditions, and the theoretical model incorporating the vapor diffusion resistance between the layer and condenser, the MOF layer temperature and water uptake profiles are also predicted (Fig. 4C). The RHs based on the MOF layer temperature before and after the solar-assisted desorption are ~65% at 25°C and ~10% at 66°C and the corresponding equilibrium water uptakes under these conditions are ~0.35 kg kg^{-1} and ~0.05 kg kg^{-1}, respectively, at a 23°C condenser temperature (estimated from fig. S6B). An amount of ~0.3 L kg^{-1} of water can be potentially harvested by saturating the MOF layer with ambient air at a solar flux below one sun.

Because of the large spacing between the layer and condenser, and the orientation of the prototype, there is a delay in desorption. Therefore, to predict the prototype water harvesting potential under equilibrium conditions, we extended the desorption time for the simulation, results of which match the prediction from the isotherm (~0.3 L kg^{-1}, shown in the upper abscissa of Fig. 4C). In order to fully utilize the steep step of water uptake in the MOF-801 isotherm, a temperature difference of ~45°C between the condenser and the layer is necessary to achieve desorption at 10% RH. For instance, if the initial RH was 20%, potentially ~0.2 L kg^{-1} can be harvested with MOF-801, which is an order of magnitude greater than that for conventional adsorbents estimated from isotherms (*29*, *30*).

REFERENCES AND NOTES

1. M. M. Mekonnen, A. Y. Hoekstra, Four billion people facing severe water scarcity. *Sci. Adv.* **2**, e1500323 (2016). doi:10.1126/sciadv.1500323 Medline
2. S. H. Schneider, *Encyclopedia of Climate and Weather* (Oxford Univ. Press, 1996).
3. R. V. Wahlgren, Atmospheric water vapour processor designs for potable water production: A review. *Water Res.* **35**, 1–22 (2001). doi:10.1016/S0043-1354(00)00247-5 Medline
4. M. Muselli, D. Beysens, J. Marcillat, I. Milimouk, T. Nilsson, A. Louche, Dew water collector for potable water in Ajaccio (Corsica Island, France). *Atmos. Res.* **64**, 297–312 (2002). doi:10.1016/S0169-8095(02)00100-X
5. O. Clus, P. Ortega, M. Muselli, I. Milimouk, D. Beysens, Study of dew water collection in humid tropical islands. *J. Hydrol.* **361**, 159–171 (2008).

doi:10.1016/j.jhydrol.2008.07.038
6. A. Lee, M.-W. Moon, H. Lim, W.-D. Kim, H.-Y. Kim, Water harvest via dewing. *Langmuir* **28**, 10183–10191 (2012). doi:10.1021/la3013987 Medline
7. R. S. Schemenauer, P. Cereceda, A proposed standard fog collector for use in high-elevation regions. *J. Appl. Meteorol.* **33**, 1313–1322 (1994). doi:10.1175/1520-0450(1994)033<1313:APSFCF>2.0.CO;2
8. O. Klemm, R. S. Schemenauer, A. Lummerich, P. Cereceda, V. Marzol, D. Corell, J. van Heerden, D. Reinhard, T. Gherezghiher, J. Olivier, P. Osses, J. Sarsour, E. Frost, M. J. Estrela, J. A. Valiente, G. M. Fessehaye, Fog as a fresh-water resource: Overview and perspectives. *Ambio* **41**, 221–234 (2012). doi:10.1007/s13280-012-0247-8 Medline
9. K.-C. Park, S. S. Chhatre, S. Srinivasan, R. E. Cohen, G. H. McKinley, Optimal design of permeable fiber network structures for fog harvesting. *Langmuir* **29**, 13269–13277 (2013). doi:10.1021/la402409f Medline
10. H. Furukawa, F. Gándara, Y.-B. Zhang, J. Jiang, W. L. Queen, M. R. Hudson, O. M. Yaghi, Water adsorption in porous metal-organic frameworks and related materials. *J. Am. Chem. Soc.* **136**, 4369–4381 (2014). doi:10.1021/ja500330a Medline
11. J. Canivet, A. Fateeva, Y. Guo, B. Coasne, D. Farrusseng, Water adsorption in MOFs: Fundamentals and applications. *Chem. Soc. Rev.* **43**, 5594–5617 (2014). doi:10.1039/C4CS00078A Medline
12. N. C. Burtch, H. Jasuja, K. S. Walton, Water stability and adsorption in metal-organic frameworks. *Chem. Rev.* **114**, 10575–10612 (2014). doi:10.1021/cr5002589 Medline
13. C. Wang, X. Liu, N. Keser Demir, J. P. Chen, K. Li, Applications of water stable metal-organic frameworks. *Chem. Soc. Rev.* **45**, 5107–5134 (2016). doi:10.1039/C6CS00362A Medline
14. J. Lee, O. K. Farha, J. Roberts, K. A. Scheidt, S. T. Nguyen, J. T. Hupp, Metal-organic framework materials as catalysts. *Chem. Soc. Rev.* **38**, 1450–1459 (2009). doi:10.1039/b807080f Medline
15. D. M. D'Alessandro, B. Smit, J. R. Long, Carbon dioxide capture: Prospects for new materials. *Angew. Chem. Int. Ed.* **49**, 6058–6082 (2010). doi:10.1002/anie.201000431 Medline
16. H.-C. Zhou, J. R. Long, O. M. Yaghi, Introduction to metal-organic frameworks. *Chem. Rev.* **112**, 673–674 (2012). doi:10.1021/cr300014x Medline
17. F. Jeremias, D. Fröhlich, C. Janiak, S. K. Henninger, Water and methanol adsorption on MOFs for cycling heat transformation processes. *New J. Chem.* **38**, 1846 (2014). doi:10.1039/c3nj01556d
18. M. F. de Lange, K. J. Verouden, T. J. Vlugt, J. Gascon, F. Kapteijn, Adsorption-driven heat pumps: The potential of metal-organic frameworks. *Chem. Rev.* **115**, 12205–12250 (2015). doi:10.1021/acs.chemrev.5b00059 Medline
19. Y. K. Seo, J. W. Yoon, J. S. Lee, Y. K. Hwang, C.-H. Jun, J.-S. Chang, S. Wuttke, P. Bazin, A. Vimont, M. Daturi, S. Bourrelly, P. L. Llewellyn, P. Horcajada, C. Serre, G. Férey, Energy-efficient dehumidification over hierachically porous metal-organic frameworks as advanced water adsorbents. *Adv. Mater.* **24**, 806–810 (2012). doi:10.1002/adma.201104084 Medline
20. M. Eddaoudi, J. Kim, N. Rosi, D. Vodak, J. Wachter, M. O'Keeffe, O. M. Yaghi, Systematic design of pore size and functionality in isoreticular MOFs and their application in methane storage. *Science* **295**, 469–472 (2002). doi:10.1126/science.1067208 Medline
21. O. M. Yaghi, M. O'Keeffe, N. W. Ockwig, H. K. Chae, M. Eddaoudi, J. Kim, Reticular synthesis and the design of new materials. *Nature* **423**, 705–714 (2003). doi:10.1038/nature01650 Medline
22. H. Furukawa, K. E. Cordova, M. O'Keeffe, O. M. Yaghi, The chemistry and applications of metal-organic frameworks. *Science* **341**, 1230444 (2013). doi:10.1126/science.1230444 Medline
23. I. Gur, K. Sawyer, R. Prasher, Searching for a better thermal battery. *Science* **335**, 1454–1455 (2012). doi:10.1126/science.1218761 Medline
24. S. Chu, A. Majumdar, Opportunities and challenges for a sustainable energy future. *Nature* **488**, 294–303 (2012). doi:10.1038/nature11475 Medline
25. See the supplementary materials.
26. J. H. Cavka, S. Jakobsen, U. Olsbye, N. Guillou, C. Lamberti, S. Bordiga, K. P. Lillerud, A new zirconium inorganic building brick forming metal organic frameworks with exceptional stability. *J. Am. Chem. Soc.* **130**, 13850–13851 (2008). doi:10.1021/ja8057953 Medline
27. S. Narayanan, S. Yang, H. Kim, E. N. Wang, Optimization of adsorption processes for climate control and thermal energy storage. *Int. J. Heat Mass Transfer* **77**, 288–300 (2014). doi:10.1016/j.ijheatmasstransfer.2014.05.022
28. S. Narayanan, H. Kim, A. Umans, S. Yang, X. Li, S. N. Schiffres, S. R. Rao, I. S. McKay, C. A. Rios Perez, C. H. Hidrovo, E. N. Wang, A thermophysical battery for storage-based climate control. *Appl. Energy* **189**, 31–43 (2017). doi:10.1016/j.apenergy.2016.12.003
29. K. Ng, H. T. Chua, C. Y. Chung, C. H. Loke, T. Kashiwagi, A. Akisawa, B. B. Saha, Experimental investigation of the silica gel–water adsorption isotherm characteristics. *Appl. Therm. Eng.* **21**, 1631–1642 (2001). doi:10.1016/S1359-4311(01)00039-4
30. H. Kim, H. J. Cho, S. Narayanan, S. Yang, H. Furukawa, S. Schiffres, X. Li, Y. B. Zhang, J. Jiang, O. M. Yaghi, E. N. Wang, Characterization of adsorption enthalpy of novel water-stable zeolites and metal-organic frameworks. *Sci. Rep.* **6**, 19097 (2016). Medline
31. D. Liu, J. J. Purewal, J. Yang, A. Sudik, S. Maurer, U. Mueller, J. Ni, D. J. Siegel, MOF-5 composites exhibiting improved thermal conductivity. *Int. J. Hydrogen Energy* **37**, 6109–6117 (2012). doi:10.1016/j.ijhydene.2011.12.129
32. S. Yang, X. Huang, G. Chen, E. N. Wang, Three-dimensional graphene enhanced heat conduction of porous crystals. *J. Porous Mater.* **23**, 1647 (2016).
33. G. Ni, G. Li, S. V. Boriskina, H. Li, W. Yang, T. J. Zhang, G. Chen, Steam generation under one sun enabled by a floating structure with thermal concentration. *Nat. Energy* **1**, 16126 (2016). doi:10.1038/nenergy.2016.126
34. A. Soleimani Dorcheh, M. Abbasi, Silica aerogel; synthesis, properties and characterization. *J. Mater. Process. Technol.* **199**, 10–26 (2008). doi:10.1016/j.jmatprotec.2007.10.060
35. R. Farrington, J. Rugh, paper presented at Earth Technologies Forum, Washington, DC, 31 October 2000 (National Renewable Energy Laboratory, 2000).
36. P. J. Cousins, D. D. Smith, H. C. Luan, J. Manning, T. D. Dennis, A. Waldhauer, K. E. Wilson, G. Harley, W. P. Mulligan, in *35th IEEE Photovoltaic Specialists Conference (PVSC 2010)* (Institute of Electrical and Electronics Engineers, 2010), pp. 275–278.
37. D. Beysens, The formation of dew. *Atmos. Res.* **39**, 215–237 (1995). doi:10.1016/0169-8095(95)00015-I
38. K. Chan, C. Y. Chao, G. Sze-To, K. S. Hui, Performance predictions for a new zeolite 13X/$CaCl_2$ composite adsorbent for adsorption cooling systems. *Int. J. Heat Mass Transfer* **55**, 3214–3224 (2012). doi:10.1016/j.ijheatmasstransfer.2012.02.054
39. İ. Solmuş, D. A. S. Rees, C. Yamalı, D. Baker, A two-energy equation model for dynamic heat and mass transfer in an adsorbent bed using silica gel/water pair. *Int. J. Heat Mass Transfer* **55**, 5275 (2012). doi:10.1016/j.ijheatmasstransfer.2012.05.036
40. M. Kaviany, *Principles of Heat Transfer in Porous Media* (Springer Science & Business Media, 2012).
41. J. R. Welty, C. E. Wicks, G. Rorrer, R. E. Wilson, *Fundamentals of Momentum, Heat, and Mass Transfer* (John Wiley & Sons, 2009).
42. T. Marshall, The diffusion of gases through porous media. *J. Soil Sci.* **10**, 79–82 (1959). doi:10.1111/j.1365-2389.1959.tb00667.x
43. P. Moldrup, T. Olesen, J. Gamst, P. Schjønning, T. Yamaguchi, D. E. Rolston, Predicting the gas diffusion coefficient in repacked soil water-induced linear reduction model. *Soil Sci. Soc. Am. J.* **64**, 1588 (2000). doi:10.2136/sssaj2000.6451588x
44. S. Sircar, J. Hufton, Why does the linear driving force model for adsorption kinetics work? *Adsorption* **6**, 137–147 (2000). doi:10.1023/A:1008965317983
45. M. Alonso, E. Sainz, F. Lopez, K. Shinohara, Void-size probability distribution in random packings of equal-sized spheres. *Chem. Eng. Sci.* **50**, 1983–1988 (1995). doi:10.1016/0009-2509(95)00061-9
46. J. O. Hirschfelder, R. B. Bird, E. L. Spotz, The transport properties of gases and gaseous mixtures. *Chem. Rev.* **44**, 205–231 (1949). doi:10.1021/cr60137a012 Medline
47. J. Crank, *The Mathematics of Diffusion* (Oxford Univ. Press, 1979).
48. R. Krishna, Describing the diffusion of guest molecules inside porous structures. *J. Phys. Chem. C* **113**, 19756–19781 (2009). doi:10.1021/jp906879d
49. J. Kärger, T. Binder, C. Chmelik, F. Hibbe, H. Krautscheid, R. Krishna, J.

Weitkamp, Microimaging of transient guest profiles to monitor mass transfer in nanoporous materials. *Nat. Mater.* **13**, 333–343 (2014). doi:10.1038/nmat3917 Medline
50. D. Beysens, Dew nucleation and growth. *C. R. Phys.* **7**, 1082–1100 (2006). doi:10.1016/j.crhy.2006.10.020
51. A. F. Mills, *Heat Transfer* (Prentice Hall, 1999).

ACKNOWLEDGMENTS

We gratefully acknowledge the support of Advanced Research Projects Agency – Energy (ARPA-E HEATS Program, Award DE-AR0000185) with R. Prasher and J. Klausner as program managers. H.K. acknowledges support from the Samsung scholarship. We thank L. Zhao at MIT Device Research Laboratory for UV-Vis-NIR spectrophotometer measurements, C. Reinhart and J. Dhariwal of MIT Sustainable Design Lab for sharing weather station data, S. Mirvakili at MIT Bio-Instrumentation Lab for pycnometer measurements, and J. Jiang for assistance at the initial stages of the work. We also thank the Institute for Soldier Nanotechnologies at MIT for use of SEM and DSC. O.M.Y. acknowledges the collaboration; valuable input, and support of Prince Dr. Turki bin Saud bin Mohammed Al-Saud (President of KACST). All data are reported in the main text and supplementary materials.

SUPPLEMENTARY MATERIALS

www.sciencemag.org/cgi/content/full/science.aam8743/DC1
Materials and Methods
Supplementary Text
Figs. S1 to S8
References (*31*–*51*)

28 January 2017; accepted 4 April 2017
Published online 13 April 2017
10.1126/science.aam8743

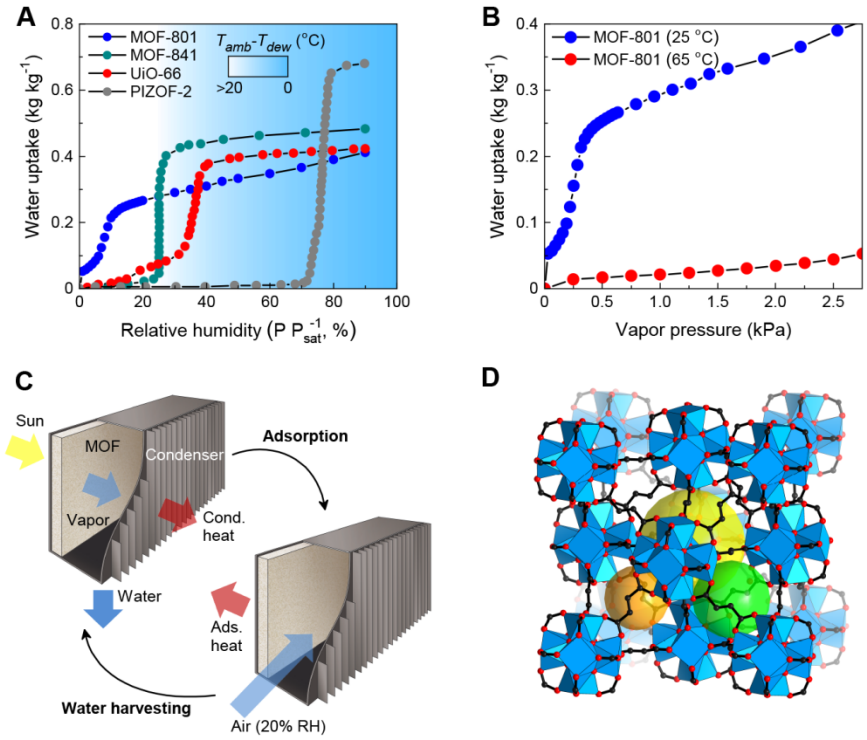

Fig. 1. Working principle of water harvesting with MOFs. (**A**) Water adsorption isotherms of Zr-based MOFs (MOF-801, MOF-841, UiO-66, and PIZOF-2) at 25°C, showing a rapid increase in adsorption capacities with a relatively small change in the relative humidity (*10*). The background color map shows the minimum temperature difference between the ambient air (T_{amb}) and the condenser (T_{dew}) required for dew collection with active cooling. (**B**) Water adsorption isotherms of MOF-801, measured at 25° and 65°C, illustrating that the temperature swing can harvest greater than 0.25 L kg^{-1} of water above 0.6 kPa vapor pressure (20% RH at 25°C). (**C**) A MOF water harvesting system, composed of a MOF layer and a condenser, undergoing solar-assisted water harvesting and adsorption processes. During water harvesting (left), the desorbed vapor is condensed at the ambient temperature and delivered via a passive heat sink, requiring no additional energy input. During water capture, the vapor is adsorbed on the MOF layer, rejecting the heat to the ambient (right). Ads. and Cond. represent adsorption and condensation, respectively. (**D**) $Zr_6O_4(OH)_4(\text{-}CO_2)_{12}$ secondary building units are linked together with fumarates to form MOF-801. The large yellow, orange and green balls three different pores. Color code: black, C; red, O; blue polyhedra, Zr.

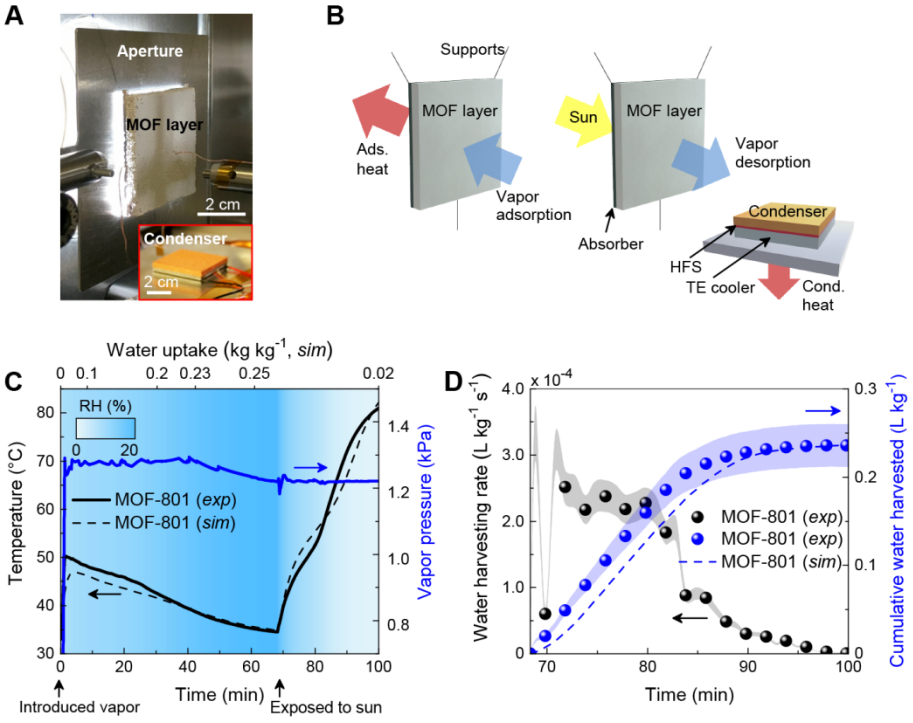

Fig. 2. Experimental characterization of harvested water from an adsorption-desorption cycle for MOF-801. (**A**) Image of MOF-801 layer and condenser. (**B**) Schematic illustrates the vapor adsorption and desorption experiments carried out under isobaric conditions. Vapor adsorbed through the sample surface by diffusion. Desorption was achieved by applying an incident solar flux on an absorber with a solar absorptance of 0.91, and the desorbed vapor was condensed simultaneously in the condenser to harvest water. The condensation heat was monitored using a heat flux sensor (HFS) with active cooling through thermoelectric (TE) cooler. Ads. and Cond. represent adsorption and condensation, respectively. (**C**) Layer temperature and chamber vapor pressure as functions of time during the water harvesting cycle. The background color map represents the estimated RH from the chamber pressure and the layer temperature, and the upper abscissa represents the predicted overall water uptake using the theoretical model as a function of time, lower abscissa. (**D**) Experimentally characterized water harvesting rate (L kg^{-1} s^{-1}) and cumulative harvested water (L kg^{-1}) during desorption. The shaded region represents the error based on uncertainties of the heat flux and MOF-801 weight measurements. The predicted temperature profile and cumulative water harvested are also included in (C) and (D), showing good agreement. The activated MOF-801 weight is 1.79 g with a layer thickness of 0.41 cm and a packing porosity (ε) of ~0.85. Subscripts sim and exp denote simulated and experimental results, respectively.

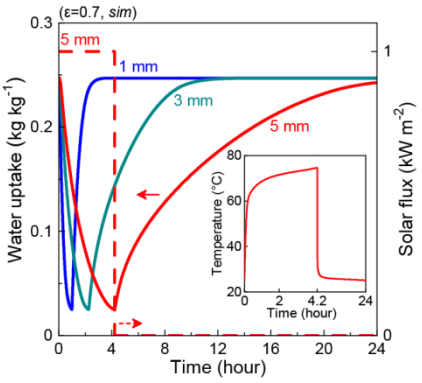

Fig. 3. Adsorption-desorption dynamics of MOF-801 in ambient air with 1 sun flux. Predicted adsorption-desorption dynamics with a packing porosity (ε) of 0.7, solar flux of 1 kW m^{-2}, and various thicknesses (1 to 5 mm). MOF-801 was initially equilibrated at 20% RH at 25°C and the partial vapor pressure rapidly increased to 100% RH at 25°C during desorption for vapor condensation. After desorption, the surrounding air-vapor mixture reverted to 20% RH. The duration of solar exposure for thicknesses of 1, 3, and 5 mm were 1, 2.3, and 4.2 hours, respectively. Note that only the duration of solar exposure for the 5-mm thick sample (red dotted line) is plotted for simplicity. The 1 mm, 3 mm, and 5 mm layers can harvest 0.08, 0.24, and 0.4 L m^{-2} of water per complete water harvesting cycle, respectively. More than 90% of the initially adsorbed water could be harvested under these conditions. Inset shows a predicted temperature profile of the 5 mm thick layer during the adsorption-desorption processes.

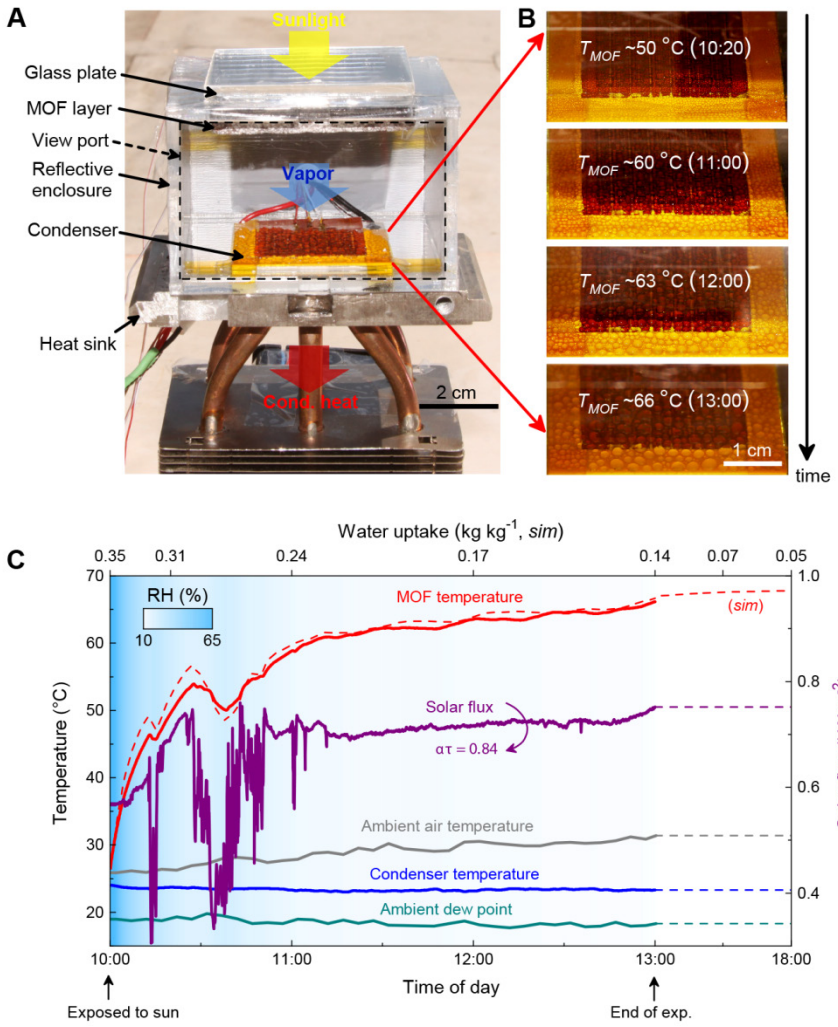

Fig. 4. Proof-of-concept water harvesting prototype. (**A**) Image of a water harvesting prototype with activated MOF-801 of weight of ~1.34 g and a packing porosity (ε) of ~0.85 with outer dimensions of 7 cm by 7 cm × 4.5 cm. (**B**) Formation and growth of droplets of water as a function of MOF temperatures (T_{MOF}) and time of day. (**C**) Representative temperature profiles for MOF-801 layer (experimental, red line; predicted, red dash), ambient air (grey line), condenser (blue line), and ambient dew point (green line), and solar flux (purple line) as functions of time of day (September 14, 2016). The background color map represents the estimated RH from the condenser saturation pressure and the layer temperature, and the upper abscissa represents the predicted water uptake using the theoretical model as a function of time, lower abscissa. Because of losses from the absorber solar absorptance (α, 0.91) and the glass plate solar transmittance (τ, 0.92), 84% of the solar flux shown in (C) was used for desorption. The layer temperature and full water harvesting potential based on complete desorption was predicted using the solar flux and environmental conditions at the end of the experiment (dash lines). The fluctuations of the solar flux during time 10:20 to 11:00 were due to the presence of clouds. Subscripts sim and exp denote simulated and experimental results, respectively.

Water harvesting from air with metal-organic frameworks powered by natural sunlight

Hyunho Kim, Sungwoo Yang, Sameer R. Rao, Shankar Narayanan, Eugene A. Kapustin, Hiroyasu Furukawa, Ari S. Umans, Omar M. Yaghi and Evelyn N. Wang (April 13, 2017)

published online April 13, 2017

Editor's Summary

Science (print ISSN 0036-8075; online ISSN 1095-9203) is published weekly, except the last week in December, by the American Association for the Advancement of Science, 1200 New York Avenue NW, Washington, DC 20005.